Received: 24 July 2024 | Accepted: 8 December 2024

DOI: 10.1002/ppj2.70016

The Plant Phenome Journal OPEN ACCESS

ORIGINAL ARTICLE

Unmanned aerial vehicle phenotyping of agronomic and physiological traits in mungbean

Shanice Van Haeften[1] | **Daniel Smith**[2] | **Hannah Robinson**[1,4] | **Caitlin Dudley**[1] | **Yichen Kang**[1] | **Colin A. Douglas**[3] | **Lee T. Hickey**[1] | **Andries Potgieter**[1] | **Scott Chapman**[2] | **Millicent R. Smith**[1,2]

[1]Queensland Alliance for Agriculture and Food Innovation, The University of Queensland, Queensland, Australia

[2]School of Agriculture and Food Sustainability, Faculty of Science, The University of Queensland, Queensland, Australia

[3]Department of Primary Industries, Queensland, Australia

[4]Department of Plant Breeding, Hochschule Geisenheim University, Geisenheim, Germany

Correspondence
Millicent R. Smith, Queensland Alliance for Agriculture and Food Innovation and School of Agriculture and Food Sustainabililty, The University of Queensland, QLD, Australia.
Email: millicent.smith@uq.edu.au

Assigned to Associate Editor Valerio Hoyos-Villegas.

Funding information
Grains Research and Development Corporation, Grant/Award Numbers: UOQ2101-003RSX, UOQ2003-011RTX; International Mungbean Improvement Network, Grant/Award Number: ACIAR;CIM2014/079; Australian Government Research Training (RTP) scholarship

Abstract

Mungbean is an important sub-tropical legume crop grown across Asia, Africa, and Australia. Yield improvement is crucial for expanding production, but phenotyping important traits across diverse environments using current approaches is challenging, limiting the scale and complexity of information captured. High-throughput phenotyping platforms offer a solution by rapidly screening traits at scale. This study deploys an unmanned aerial vehicle (UAV) platform to determine the potential of phenotyping a range of agronomic and physiological traits within a diverse mungbean population evaluated across three field trials. Three predictive data-driven modeling approaches were undertaken to evaluate performance accuracy in predicting these traits: linear regression, stepwise regression, and partial least squares regression. Results show that using the geometric trait "coverage" as a proxy is most suitable for screening visual traits like early vigor. For functional traits (i.e., aboveground biomass), predictive data-driven models demonstrate high accuracy during early- and mid-canopy development stages (R^2 0.79, root mean square error [RMSE] 4.08 and R^2 0.8, RMSE 26.92, respectively), but accuracy declines in late-canopy development (R^2 0.33 and RMSE 43.15). Prediction accuracy can be optimized by using different modeling approaches at different stages during the transition from early- to mid-canopy development as well as canopy closure. Similar findings were observed when examining the prediction models for the physiological trait, stomatal conductance (R^2 0.69 and RMSE 0.10). These approaches are expected to enable breeders and researchers to incorporate UAV-based phenotyping systems into mungbean improvement programs. Such approaches might be most efficiently used at scale if applied as part of a "real-time" calibration approach.

Abbreviations: DEM, digital surface elevation model; GCP, ground control point; LM, linear regression model; NDRE, normalized difference red edge; NDVI, normalized difference vegetation index; OSAVI, optimized soil-adjusted vegetation index; PLS, partial least squares; RMSE, root mean square error; SWR, stepwise multilinear regression; UAV, unmanned aerial vehicle; VI, vegetative index; VIF, variation inflation factor.

1 | INTRODUCTION

Mungbean [*Vigna radiata* (L.) R. Wilzeck var. *radiata*] is a significant cash and food crop globally, occupying over 6 million ha (Kim et al., 2015). Mungbean has a short growing duration, making it an ideal rotation crop for inclusion in a wide range of subtropical farming systems. Australian mungbean production has steadily grown in the past three decades from an average of 17,583 tonnes across 33,325 ha between 1990 and 1995 to 107,318 tonnes across 89,297 ha between 2015 and 2021 (ABARES, 2020). Demand is expected to increase significantly over the next decade with the increased interest in the plant-based protein sector (Colgrave et al., 2021). Despite the nutritional and economic value of mungbean becoming more apparent (Nair & Schreinemachers, 2020), mungbean expansion in Australia is constrained by yield variability across seasons (Y. S. Chauhan & Williams, 2018; Rachaputi et al., 2019). This is a result of susceptibility to abiotic and biotic stresses and physiological constraints that could be optimized to improve productivity under different production scenarios (Van Haeften et al., 2023). Consequently, concerted efforts are underway to identify new genetics for important agronomic and physiological traits that could support and improve productivity across different production environments (Australian Centre for International Agricultural Research (ACIAR), 2022; Sandhu & Singh, 2020).

In crop improvement programs, field-based phenotyping is key to assess and characterize trait value and trait relationships that underpin productivity at a single plant- or canopy-scale (Pieruschka & Schurr, 2019). However, current field-based phenotyping methods for traits such as vigor, aboveground biomass, and plant height often require manual collection of data, and are labor intensive, costly, and prone to subjectivity, as well as potentially destructive to plants (Borra-Serrano et al., 2020; Potgieter et al., 2018). For example, harvest index is a key trait in mungbean as it is associated with efficient conversion of resources to grain yield (Collins et al., 2019; M. R. Smith et al., 2018). However, one of the major components of estimating harvest index is total aboveground biomass accumulation, which due to the phenotyping challenges, makes it difficult to evaluate this trait at a large scale across multiple environments. There are also many other key physiological traits that contribute to yield potential and adaptation to abiotic stress that cannot be captured by eye or efficiently at a large scale. For instance, canopy temperature is linked to water use efficiency, particularly under water-limiting environments (Conaty et al., 2015; Condon et al., 2004). These limitations create a phenotyping bottleneck, which can ultimately restrict the scale of experiments across environments and limit the number of genotypes examined (Furbank et al., 2019; Potgieter et al., 2018). This bottleneck is further pronounced as advances in gene sequencing technology have increased the availability of genomic information, which requires connectivity with phenotypic data to be able to connect the plant's genetic makeup with an observable characteristic that could be optimized for crop improvement.

Core Ideas

- Unmanned aerial vehicle (UAV)-derived coverage serves as a useful proxy for early vigor, surpassing traditional scores in resolution and accuracy.
- Prediction of aboveground biomass can be optimized by applying different prediction models across crop development.
- UAV-derived imagery can phenotype canopy traits unable to be visually assessed, such as stomatal conductance.

The recent development of high-resolution sensors onboard unmanned aerial vehicle (UAV) platforms offers the opportunity to overcome many of the challenges associated with traditional phenotyping methods, due to their ability to rapidly capture accurate, non-destructive measurements at a large spatial and temporal scale (Chapman et al., 2014; Hassan et al., 2018; D. T. Smith et al., 2021). A range of sensors can be placed onboard these platforms, for instance, multispectral and hyperspectral sensors, to capture high-resolution data that may not be captured from the ground. The reflectance data captured by multispectral and hyperspectral sensors allow for the determination of vegetative indices (VIs) that are used as a proxy for vegetation classification and plant productivity estimates (e.g., Brunner et al., 2024; Selvaraj et al., 2020). Additionally, digital surface models can be generated, which allow researchers to capture additional physiological traits such as plant height and volume, which have been shown to improve prediction accuracy of complex traits such as aboveground biomass (Bendig et al., 2015; Hassan, Yang, Fu et al., 2019; Yue et al., 2017).

Recent studies exploring UAV-derived data have successfully evaluated a range of morphological and physiological traits in many major crops such as sorghum (e.g., Gano et al., 2021), wheat (e.g., Aparicio et al., 2000), maize (e.g., Vina et al., 2004), and soybean (e.g., Crusiol et al., 2019). Further complex approaches have utilized plant height, plant width and two VIs, normalized difference vegetation index (NDVI), and normalized difference red edge (NDRE) index to estimate aboveground biomass with high precision in common bean (Barboza et al., 2023) and predicted radiation use efficiency in wheat by using VIs within partial least square models (Robles-Zazueta et al., 2021). In mungbean specifically, UAV-based phenotyping is emerging but limited. A recent study demonstrated the potential of this technology

by successfully linking fractional canopy cover and VIs with light interception and aboveground biomass across multiple vegetative stages in three mungbean cultivars (Xiong et al., 2023). While traditional ground-based phenotyping approaches in mungbean have provided invaluable insight into the mechanisms that drive yield development (Geetika, Hammer et al., 2022, Geetika, Collins et al., 2022), the application of UAV imagery platforms in related legume crops and the recent mungbean UAV study showcase the promising results of increasing accuracy and precision of data collection across a larger scale, as well as measuring unexplored traits, while reducing cost and labor requirements.

We expand this approach further in mungbean and predict a range of traits across vegetative and reproductive stages in diverse mungbean pre-breeding germplasm. Therefore, this study aims to explore the potential of utilizing UAVs mounted with a multispectral sensor to phenotype several types of agronomic traits (visual, functional, and physiological), including early vigor, aboveground biomass, and stomatal conductance, in diverse mungbean accessions grown across multiple environments. Using the multispectral sensor, this study will identify key VIs and geometric traits that can be used to predict traits of interest for utilization in crop improvement programs.

2 | MATERIALS AND METHODS

2.1 | Plant material and field trial design

This study was conducted using a mungbean nested association mapping (NAM) population previously developed by the Queensland Department of Primary Industries (DPI) and the Queensland University of Technology (Noble, 2017). The population of 2060 lines was developed using 31 donor parents, which covered known genetic and phenotypic diversity for phenology, architecture, grain size, and grain yield. In addition, a diversity panel was also studied, which included the NAM parents, five Burmese cultivars that are widely growth throughout southern Asia, as well as a blackgram (*Vigna mungo*) cultivar, Onyx-AU. Accessions AGG 325964 (M10403), AGG 325968 (M12130), AGG 325973 (M11238), 68 AGG 325977 (M08019), and AGG 325976 (Maus12-053) are co-owned by DPI and the Grains Research and Development Corporation.

A subset of the NAM population, as well as the NAM parents and additional lines, was sown in 2022 and 2023 at the Pacific Seeds Foundation Farm, Allora (Allora22–28.06 ˚S; 151.96 ˚E) and The University of Queensland (UQ) Gatton Campus (Gatton22–28.06 ˚S; 151.96 ˚E). An additional trial undertaken in 2023 also at UQ Gatton Campus (Gatton23) was sown with just the NAM parents (Table 1). Allora22 and Gatton22 were grown under rainfed conditions with no supplementary irrigation, whereas Gatton23 was irrigated. These

TABLE 1 Summary of site information for field trials examined in this study.

Trial	Year	Location	Location GPS	Sowing date	Trial design	In-crop rainfall (mm)	Plant material	Genotype number
Allora22	2022	Allora (QLD)	28.06 ˚S; 151.96 ˚E	Jan. 21	Partial replication (four replicates diversity panel; two replicates NAM subset) 4-m × 1.52-m plots Two rows 25 plants/m^2	457.6	Diversity panel NAM subset	387
Gatton22	2022	Gatton (QLD)	27.55 ˚S; 152.33 ˚E	Feb. 1	Partial replication (four replicates diversity panel; two replicates NAM subset) 4-m × 1.52-m plots Two rows 25 plants/m^2	644.2	Diversity panel NAM subset	392
Gatton23	2022	Gatton (QLD)	27.55 ˚S; 152.33 ˚E	Dec. 22	Four replications 4-m × 1-m plots Two rows 25 plants/m^2	187.8	Diversity panel	33

Abbreviation: NAM, nested association mapping.

TABLE 2 Summary of flights captured in this study corresponding to the ground-based measurement captured.

	Allora22		Gatton22		Gatton23	
Trait	**Date**	**DAS**	**Date**	**DAS**	**Date**	**DAS**
Vigor	Feb. 10	20	Feb. 22	21	Jan. 10	19
Aboveground biomass (vegetative)	NA	NA	NA	NA	Jan. 25	34
Aboveground biomass (flowering)	Mar. 16	54	Mar. 22	49	Feb. 13	53
Aboveground biomass (podding)	Apr. 12	81	Apr. 19	77	Mar. 9	77
Stomatal conductance (reproductive development)	Mar. 16	54	Apr. 5	63	NA	NA

Note: Date of flight and days after sowing (DAS) are presented. NA, measurement not captured for that particular trait at that specific trial.

trials used a partially replicated design where the diversity panel was replicated four times and NAM lines were replicated twice. All germplasm was planted in two rows with a 0.76 m row spacing in Allora22 and Gatton22. Plot length varied with location where Gatton22 had 4-m plots and Allora had 3.5-m plots. In Gatton23, germplasm was sown in a randomized block design within two rows in 4-m × 1-m plots (0.5 m row spacing). All trials were sown in model-based row-column design using genetic relatedness (Cullis et al., 2020), which was implemented using the R statistical package "od" (https://mmade.org/optimaldesign/).

Consistent management was applied across all trials including inoculation of seeds at sowing with Group I inoculum (EasyRhiz, New Edge Microbials Pty. Ltd.) and basal application of Starter Z fertilizer at a rate of 25 kg ha^{-1}. Field trials were monitored regularly throughout the growing season for pest, disease, and weed presence. Appropriate herbicide, fungicide, and pesticide applications were implemented promptly at the first sign of pest pressure or disease symptoms as recommended by industry standards (GRDC, 2017) to ensure optimal plant growth and development. In addition, all weeds were manually removed, when required, to ensure trials were free of weeds at the time of each UAV flight.

2.2 | Ground-based measurements

2.2.1 | Early vigor visual scoring

Early vigor refers to the rapid development of leaf area at the early stage of the crop's development. High early vigor has been shown to improve weed competitiveness, which is of value to mungbean production systems (Bertholdsson, 2005; Rebetzke & Richards, 1999). Across all four trials, early vigor was captured by recording a 1–9 visual score 2 weeks after sowing, with 1 denoting the most vigorous phenotype (larger plants with greater coverage and biomass) and 9 denoting the least vigorous phenotype (smaller plants with reduced coverage and biomass) (Table 2). The vigor score incorporates multiple plant characteristics including ground coverage, plant height, and overall plant robustness, providing a composite assessment of early-stage plant development and this visual scoring system is the established standard in breeding programs (Kipp et al., 2014; Nguyen et al., 2018). To ensure scoring consistency, reference cultivars (Crystal and Celera II-AU) with known high and low vigor characteristics were used as benchmarks to anchor the scoring scale across trials.

2.2.2 | Aboveground biomass

Canopy structure as well as canopy development is critical for crops to intercept the light required to support growth and productivity (Hikosaka, 2005). Further, understanding how the plant remobilizes resources from aboveground biomass to yield components is critical in improving grain yield. Aboveground biomass cuts were performed on the diversity panel at two growth stages (mid- and late-canopy development) across all field trials with the early-development stage also captured at Gatton23 only (1.52 m × 0.5 m in Allora22 and Gatton22; 1 m × 0.5 m in Gatton23). The number of plants within each cut was recorded, and biomass dried for 7 days at 65°C and weighed for total aboveground biomass dry weight.

2.2.3 | Stomatal conductance

Stomatal conductance refers to the rate of diffusion through the stoma and is a key indicator of photosynthetic capacity and water use efficiency (Bertolino et al., 2019). Stomatal conductance at reproductive development in Allora22 and Gatton22 was captured for the diversity panel using a LI-600 porometer (LI-COR Inc). To standardize measurements and minimize diurnal variation effects, all measurements were consistently captured from 10:00 a.m. to 12:00 p.m. Measurements were taken from the same section of the plot that

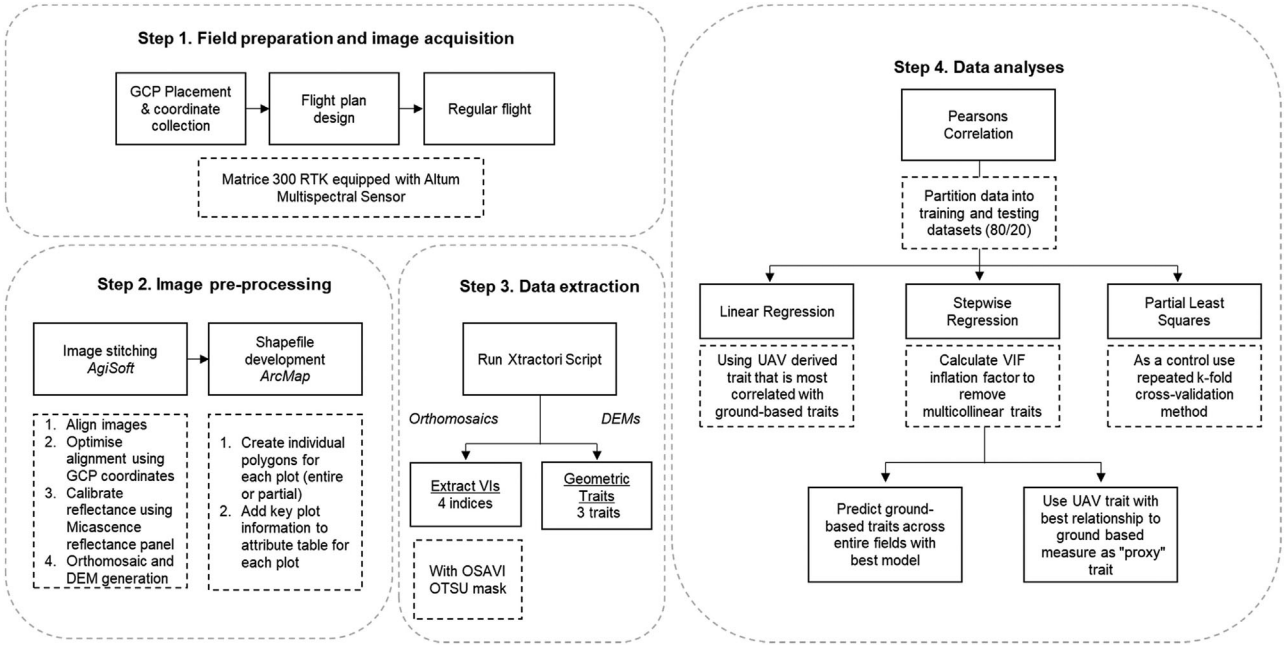

FIGURE 1 Workflow schematic representing methodology for unmanned aerial vehicle (UAV) data processing and modeling for trait prediction. DEM, digital surface elevation model; GCP, ground control point; OSAVI, optimized soil-adjusted vegetation index; VI, vegetative index; VIF, variation inflation factor.

was captured for biomass cuts (1.52 m × 0.5 m in Allora22 and Gatton22; 1 m × 0.5 m in Gatton23). For each plot, measurements were sequentially repeated three times on the topmost fully expanded leaf for five randomly selected plants within the plot. This standardized and replicated sampling approach helped to capture natural variation in stomatal conductance under field conditions, allowing for a diverse dataset for calibration.

2.3 | UAV sensing data processing and collection

2.3.1 | UAV campaign

The workflow involved four phases: (1) field preparation and image acquisition, (2) image pre-processing, (3) data extraction, and (4) data analyses (Figure 1). Images were captured using a MicaSense Altum sensor (MicaSense Inc.) mounted on the Matrice 300 RTK (DJI) UAV platform, which was flown over the field trials on the day that corresponded with the respective ground-based measurement (Table 2). Flights were captured during sunny, cloud-free conditions between 10:00 a.m. and 12:00 p.m. The Altum sensor captured images across six spectral bands: blue (475 ± 32 nm), green (560 ± 27 nm), red (668 ± 14 nm), red edge (717 ± 12 nm), near infrared (842 ± 57 nm), and long-wave thermal infrared (11 ± 6 μm). Prior to the first flight, between 7 and 8 ground control points (GCPs) were placed around the borders of the trial as well as uniformly inside the trial using Propeller AeroPoints (Propeller Aerobotics Pty Ltd.) to provide positional accuracy of the UAV images captured. The UAV and camera were flown across the trials at an altitude of 20 m with 80% side and frontal image overlap and a pixel size of 0.86 cm and 13.5 cm for the multispectral and thermal bands, respectively. Before and after the commencement of each individual flight, an image of a calibrated reflectance panel (MicaSense Inc.) was captured to correct the imagery based on the light conditions during the flight time.

2.3.2 | Image pre-processing

Using a customized Python script originally developed by Das et al. (2022) and further developed by one of the authors (Daniel Smith), raw images captured were stitched together to generate a geo-referenced orthomosaic and digital surface elevation model (DEM) using the software AgiSoft (Agisoft LLC) (D. T. Smith et al., 2024). This process involves aligning the images together, using the AeroPoints ground control reference points (GCPs) that have centimeter-level accuracy (Propeller) and calibrating the reflectance values based on the calibration panel. Several plot boundaries across each site were generated using ArcMap (Esri), with the size and placement of the shapefiles being determined by the ground-based measurement protocols for each trait type examined (.shp format). For the visual assessment of early vigor, which evaluated the entire plot, shapefiles encompassed the complete plot

TABLE 3 Remote sensing traits investigated in this study.

Remote sensing trait	Calculation	Reference
OSAVI (optimized soil-adjusted vegetation index)	$(1 \times 0.16) \times \frac{(NIR - RED)}{(NIR + RED + 0.16)}$	(Rondeaux et al., 1996)
NDVI (normalized difference vegetation index)	$\frac{(NIR - RED)}{(NIR + RED)}$	(Rouse et al., 1974)
NDRE (normalized difference red edge)	$\frac{(NIR - RED\ EDGE)}{(NIR + RED\ EDGE)}$	(Fitzgerald et al., 2006; Li et al., 2018)
Thermal band	THERMAL BAND	(Tunca et al., 2023)

area. For the physiological and destructive traits (i.e., stomatal conductance and aboveground biomass), measurements were captured from small subsections at the plot ends and smaller shapefiles were generated to specifically cover these sampling areas. For each individual plot boundary detailed plot descriptions including crop name, genotype, pedigree, plot ID, row spacing, and sowing density were attached, which is required for the software used for the extraction of sensing data.

2.3.3 | Extraction of sensing data from multispectral and RGB imagery

VIs, canopy cover, and geometric traits (i.e., height and volume) were extracted using *Xtractori*, which is a python environment-based program developed by UQ to extract indices from five- and six-layer multispectral cameras (Das et al., 2022) (Table 3). This program extracts a range of VIs and canopy traits from the orthomosaic by first distinguishing plant material from soil background using a masking approach. This approach utilizes the optimized soil-adjusted vegetation index (OSAVI) along with the Otsu's thresholding method to separate green plant matter (D. T. Smith et al., 2024). The Otsu's method automatically determines an optimal OSAVI threshold value (OSAVIthreshold) selected based on a discriminant criterion by maximizing the between-class variance between plant and soil pixels (Otsu, 1979). Pixels with OSAVI values above this threshold were classified as plant material (OSAVI > OSAVIthreshold), while those below this threshold were classified as soil background (OSAVI < OSAVIthreshold). The effectiveness of this approach is demonstrated visually in Figure S1, which shows the progression from original image to final segmentation.

Seven UAV-derived traits (VIs and geometric traits) were extracted for examination in this study, including OSAVI, NDVI, NDRE, and the thermal band (Table 3). Coverage was also calculated by Otsu thresholding by estimating the proportion of pixels within plot boundary that are denoted plant material. Additionally, two geometric traits were extracted from the DEM orthomosaic. Height was calculated by subtracting the digital terrain model (ground elevation from emergence flight) from the crop surface model (top of canopy surface at each imaging timepoint). The digital terrain model provided baseline ground elevation, while, date-specific crop surface models captured crop development over time. The 98th percentile of these height values was used as the representative plant height for each plot, due to its previous strong relationship with ground-based plant height (Malambo et al., 2018; Wang et al., 2022). Volume was calculated as the sum of pixel heights within each plot multiplied by the ground sample distance (pixel size), then standardized by dividing by the plot area to enable cross-site comparisons (Maimaitijiang et al., 2019; D. T. Smith et al., 2024). The thermal data were standardized by subtracting the thermal value from the air temperature and then dividing by vapor pressure deficit.

3 | STATISTICAL ANALYSES

3.1 | Predictive modeling

To understand the association between the ground-based and aerial-based traits, a traditional Pearson product-moment correlation was undertaken using plot-level data. Three approaches were then undertaken to identify the most appropriate prediction model for each trait. For all approaches, the dataset for each trait from each trial was split where 80% was used for training the models and 20% used as a validation set for evaluating the model performance. To ensure a balanced representation of trait variation across experiments, the training and validation datasets were stratified by both the range of trait values and the experiment they originated from. All data for aboveground biomass were combined and partitioning was undertaken on all datapoints, excluding aboveground biomass determined at the vegetative stage as these data were only collected from one site and serve as an initial exploration of aboveground biomass prediction for this stage.

The first approach was a simple linear regression model (LM), which was fitted using the UAV-derived traits that were found to be the most significantly correlated across all trials. The second approach was a stepwise multilinear regression (SWR) using both the VIs and geometric traits. This

approach was undertaken using the "MASS" package in R and involves iteratively adding and removing predictor variables in the model to identify a subset of these variables that best predicts the trait and reduces prediction error. As this approach cannot handle multicollinearity in variables, an initial step was undertaken to reduce the number of variables that had high collinearity with others (Zhi et al., 2022). The variation inflation factor (VIF) was used to select traits with reduced multicollinearity. A higher VIF indicates greater multicollinearity, and a VIF value less than 10 is considered acceptable (Thompson et al., 2017). After subsetting these variables, Akaike information criterion was used in the stepwise regression to determine the model with the best fit (Yamashita et al., 2007).

The third approach was a partial least squares (PLS) regression method, which is a multivariate analysis used widely due to its ability to manage collinearity across traits using dimension reduction techniques. This approach was undertaken using the "caret" package in R. The model was tuned to find the optimal number of components "ncomps" that were needed to be incorporated. The data were also transformed to be centered and scaled using the "preprocess" function in the package. A *k*-fold cross-validation method was undertaken on the training dataset as a resampling method to estimate the performance of the model. This approach divides the data into several folds, which are used to estimate the error rate of machine learning-based classifications on iteration and outputs the final model with the least error rate. In this study, we used five folds and 10 repetitions.

After developing the models for all three approaches, they were then evaluated on the validation dataset. The performance of these approaches was then assessed by evaluating the coefficient of determination (R^2), which represents the fraction of the trait variance explained by the model, and the root mean square error (RMSE), which captures the average magnitude of error.

3.2 | Spatial analyses

Spatial analyses were conducted for the predicted values for each trait, in addition to the early vigor scores, to correct for spatial heterogeneity within each trial. A systematic model building approach was implemented using ASReml-R, to fit a linear mixed model to estimate the best linear unbiased estimates (BLUEs) (Butler et al., 2009). The base model included plot-level trait observations and genotype as fixed effects, with block fitted as a random effect. A separable autoregressive process of order one (AR1 × AR1) was fitted as a residual variance structure to account for spatial correlation. Additional spatial terms were systematically evaluated to optimize the model for each trait. These included linear column and linear row effects as fixed effects, and column and row as random effects. The significance of each additional term was assessed using Wald chi-squared tests for fixed effects and likelihood ratio tests for random effects. Terms were only retained in the final model if they significantly improved model fit ($p < 0.05$). The specific spatial terms retained for each trait's final model are detailed in Table S1. The broad-sense heritability (H^2) of each trait was also determined using the following equation:

$$H^2 = 1 - \frac{A_{tt}}{(2\gamma_v)},$$

where A_{tt} is the average prediction error variance and γ_v denotes the genetic variance (Cullis et al., 2006).

TABLE 4 Pearson correlation coefficient (*r*) between UAV-derived traits (VIs and geometric traits) and early vigor scores across three field trials (Allora22, Gatton22, and Gatton23).

	Allora22	Gatton22	Gatton23	All trials
NDRE	−0.52	−0.27	−0.3	−0.17
NDVI	−0.53	−0.35	−0.72[a]	−0.2
OSAVI	−0.54[a]	−0.32	−0.68	−0.17
Thermal	0.52	0.22	0.29	0.01
Coverage	−0.37	−0.42[a]	−0.69	−0.23[a]
Height	−0.42	−0.29	−0.64	−0.08
Volume	−0.22	−0.08	−0.26	−0.01

Abbreviations: NDRE, normalized difference red edge; NDVI, normalized difference vegetation index; OSAVI, optimized soil-adjusted vegetation index; UAV, unmanned aerial vehicle; VI, vegetative index.

[a]Vegetative index or geometric trait used for linear regression model.

4 | RESULTS

4.1 | Vegetative indices can be used as a proxy trait to phenotype early vigor

Across all sites, all traits were negatively correlated with early vigor, excluding thermal, which was positively correlated (Table 4). The UAV-derived trait, coverage, overall had a strong correlation with early vigor across sites. In Allora22, OSAVI had the strongest correlation with early vigor (R^2 −0.54), whereas in Gatton22, coverage had the strongest association (R^2 −0.42), and in Gatton23, NDVI had the strongest association (R^2 -0.72).

Based on correlation analyses, the UAV-derived trait that had the strongest correlations to early vigor across the three sites was fit in an LM (Figure 2a). Across each individual site using this approach with the predictor OSAVI for Allora22, coverage for Gatton22 and NDVI for Gatton23 generated low- to moderate-performing prediction models (Allora22: R^2 0.29, RMSE 1.37; Gatton22: R^2 0.25, RMSE 1.40; and Gatton23: R^2 0.60, RMSE 1.01). To test whether

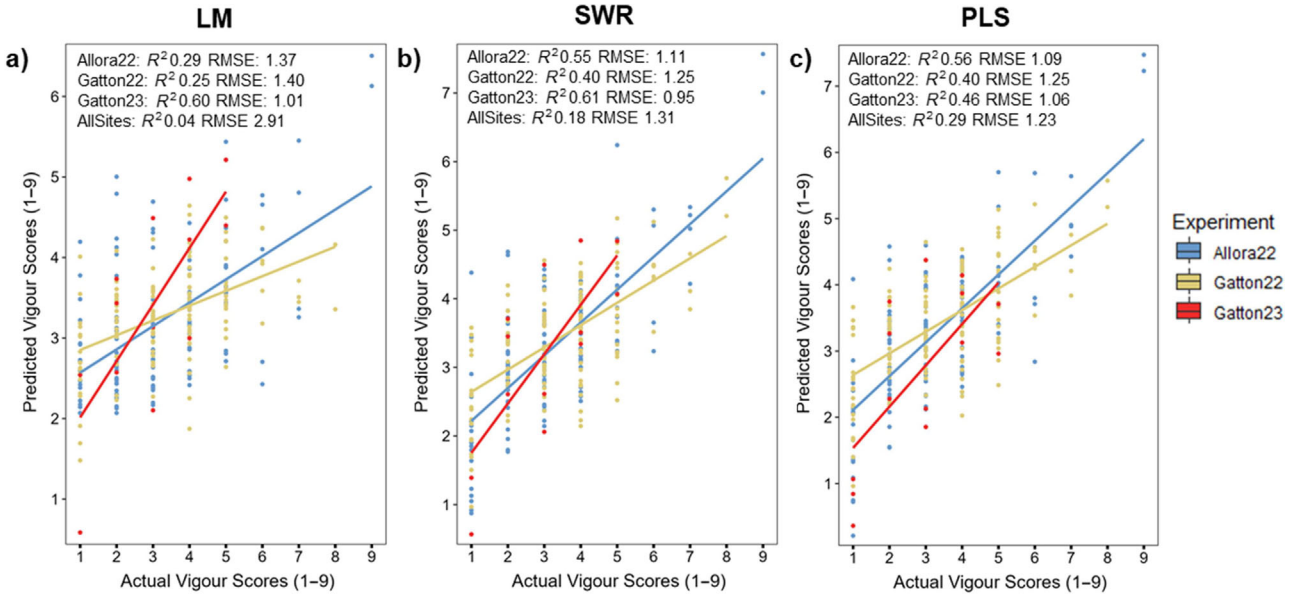

FIGURE 2 Predicted and actual vigor scores (1–9) for diverse mungbean genotypes grown across three environments: Allora22 (blue), Gatton22 (yellow), and Gatton23 (red) and all trials combined using (a) linear regression model, (b) stepwise regression model, and (c) partial least squares (PLS) model. Model performance indicators (R^2 and root mean square error [RMSE]) for each site are presented. LM, linear regression model.

combining data across sites could improve predictions, the three types of prediction models were tested using the complete dataset (all environments included). However, this combined-site approach using coverage as a predictor for the LM model showed reduced accuracy (R^2 0.04, RMSE 2.91) compared to site-specific models. A multivariate approach (stepwise regression) and a machine learning regression approach (PLS) was undertaken to understand whether a combination of VIs and geometric traits could improve prediction accuracy (Figure 2b,c; Table S2; Figure S2). Accuracy of SWR models for Allora22, Gatton22, Gatton23, and all sites showed low to moderate performance (Allora22: R^2 0.55, RMSE 1.11; Gatton22: R^2 0.4, RMSE 1.25; and Gatton23: R^2 0.61, RMSE 0.95), with similar lower prediction accuracy when data from all sites were combined (all sites: R^2 0.18, RMSE 1.31). For Allora22, the predictors used in the model were thermal, NDRE, coverage, and volume. For Gatton22, the predictors were coverage, NDVI, height, volume, and thermal. For Gatton23, the predictors were OSAVI, coverage, and NDRE, and for all sites, they were coverage, OSAVI, volume, and thermal. This was similarly observed when examining the PLS models, whereby the main contributing predictors in the model for each site were OSAVI, thermal, NDVI, and NDRE for Allora22; height and coverage for Gatton22; and height, coverage, NDVI, and OSAVI for Gatton23 and thermal for all sites (Allora22: R^2 0.56, RMSE 1.09; Gatton22: R^2 0.4, RMSE 1.25; Gatton23: R^2 0.46, RMSE 1.06; and all sites: R^2 0.29, RMSE 1.23). This suggests that prediction models may not be the most appropriate approach for this trait. Using coverage, which was the most correlated with early vigor across

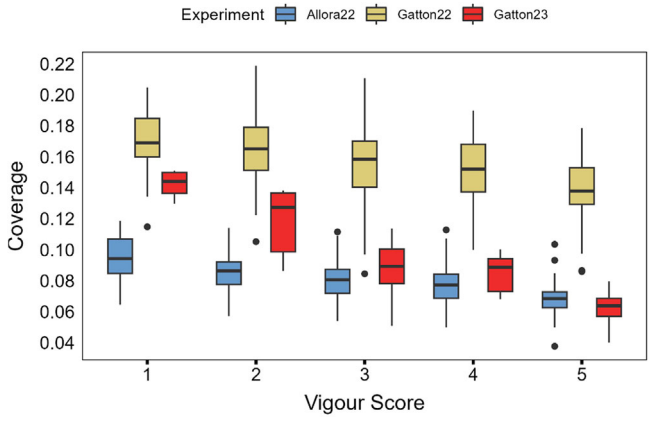

FIGURE 3 Best linear unbiased estimates (BLUEs) for coverage values captured across the mungbean diversity panel at Allora22 (blue), Gatton22 (yellow), and Gatton23 (red). Coverage values of genotypes were grouped by the BLUEs of the visual scores that were captured with only scores 1–5 being presented. With 1 denoting the most vigorous genotypes (larger plants with greater coverage and biomass) and 5 denoting the less vigorous genotypes (smaller plants with reduced coverage and biomass).

all trials, would be more appropriate to use as a "proxy" trait for this ground-based visual measure.

Using coverage across each site as a proxy for early vigor, substantial genotypic variation in early vigor was observed across sites (Allora22: 0.04–0.12, Gatton22: 0.08–0.22, and Gatton23: 0.03-0.16). Early vigor also differed with environment where Allora22 recorded the lowest values, followed by Gatton23 and Gatton22 (Figure 3). Genotypes that were

TABLE 5 Broad-sense heritability (H^2) of early vigor visual scores and coverage across three field trials.

Traits	Allora22	Gatton22	Gatton23
Early vigor score (1–9)	0.67	0.74	0.84
Coverage	0.68	0.85	0.93

recorded using traditional scoring as the most vigorous and least vigorous were similar across sites. However, the genotypic differences were more pronounced when using coverage as a proxy compared to traditional visual scoring (Figure 3). Only scores 1–5 are presented as these were the scores recorded across all three trial sites, enabling direct cross-site comparisons of genotypic variation in early vigor. Specifically, genotypes that have a low vigor score in Allora22 and Gatton22 had a coverage value that would suggest a higher vigor value and vice versa than determined from visual scoring. Several genotypes were also observed to have higher vigor values compared to the commercial cultivar Crystal (0.06–0.15), including AGG 325966 (0.12–0.17), Berken (0.10–0.19), Black Berken (0.1–0.19), and AGG 325968 (0.1–0.17) (Table S3).

When comparing the broad-sense heritability of these two approaches, the UAV-derived trait showed a higher heritability across all three sites (Table 5), suggesting that coverage can provide a more informative and reliable assessment of the genetic variation of early vigor in the field.

4.2 | Different UAV traits can be used to predict biomass across growth stages

Across all growth stages, significant associations were determined between UAV-derived traits and total aboveground biomass (Table 6). During the early-canopy development stage, coverage (R^2 0.9) had the strongest positive relationship with biomass, and for mid-canopy development stage, height had the strongest positive relationship (R^2 0.73). Comparatively, for late-canopy development, coverage had a strong relationship with aboveground biomass although, this relationship was moderate in association (R^2 0.41).

All models predicted aboveground biomass with a high accuracy at the early-canopy development stage (Figure 4a–c). The LM approach using coverage recorded the highest prediction accuracy (R^2 0.79, RMSE 4.08), followed by the PLS approach where the main contributing predictor was coverage, and the SWR approach using the predictor variables volume, thermal, and height (R^2 0.76, RMSE 4.85 and R^2 0.73, RMSE 4.89, respectively). Similarly, all models for predicting biomass at the mid-canopy development stage also performed well (Figure 4d–f). In this case, the SWR approach (predictors: height, thermal, NDRE, and coverage) recorded the highest accuracy (R^2 0.80, RMSE 26.92), followed by the PLS approach (main contributing predictors: height, NDRE, and OSAVI) (R^2 0.79, RMSE 28.01) and the LM approach using height (R^2 0.68, RMSE 36.50) (Table S2; Figure S3). When examining the models for predicting biomass at the late-canopy development stage the prediction accuracy for all models reduced significantly (Figure 4g–i). The SWR model performed best at this stage using the predictors coverage and NDVI (R^2 0.33, RMSE 43.15), followed by the LM approach using coverage (R^2 0.30, RMSE 82.90), and finally the PLS approach with the main contributing predictors of coverage, NDVI, OSAVI, volume, and NDRE (R^2 0.26, RMSE 45.76).

Models were applied to UAV traits from every plot to predict total aboveground biomass at each developmental stage (early-, mid-, and late-canopy development), and spatial analyses were undertaken to calculate BLUEs (Figure 5). Significant phenotypic variation was observed across all stages and environments. Across all stages, Gatton23 had the highest predicted biomass compared to all three sites (Figure 5a–c). During early- and mid-canopy development stages, Allora22 had higher predicted biomass compared to Gatton22; however, as the plants developed and reached the late-canopy development stage, a higher total biomass was recorded at Gatton22 compared to Allora22. The broad-sense heritability for predicted biomass across all growth stages and all sites was high (H^2 0.65–0.87).

The amount of aboveground biomass produced by commercial cultivar Crystal in comparison to other NAM parents varied across the environments and development stages (Table S4). For example, during the early-development stage in Allora22, Crystal produced a low amount of aboveground biomass (14.14 ± 0.82 g) compared to 24 other NAM parents (15.63–24.95 g). However, in Gatton22 and Gatton23, Crystal produced a moderate amount of biomass (16.34 ± 0.84 and 58.7 ± 3.51, respectively) compared to most other NAM parents with only eight genotypes producing higher biomass in both Gatton22 (16.93–20.13 g) and Gatton23 (59.03–68.87 g), respectively. A similar trend was observed for aboveground biomass at the mid- and late-canopy development stage.

4.3 | A combination of thermal, VIs, and geometric traits can be used to estimate stomatal conductance

Several indices were determined to have a strong correlation with stomatal conductance (g_{sw}) at the reproductive stage (Table 7) where thermal had the strongest correlation (R^2 0.79), followed by NDRE (R^2 0.74).

By utilizing the three prediction model approaches at reproductive development, it was observed that the PLS approach

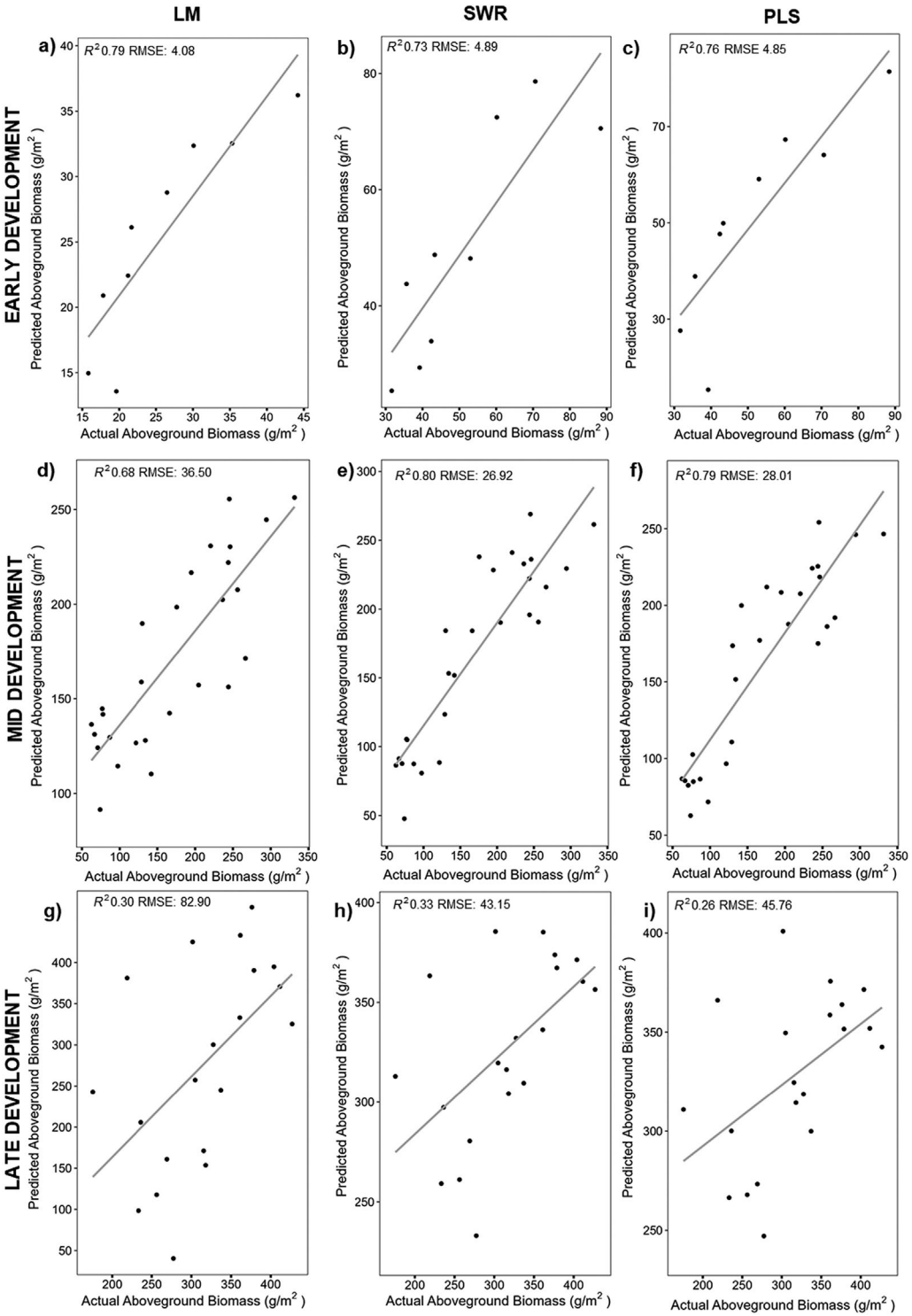

FIGURE 4 Predicted and actual aboveground biomass (g/m^2) at the plot level on the validation dataset for mungbean genotypes grown across three environments combined (Gatton22, Allora22, and Gatton23) using different prediction models: (a) linear regression model, (b) stepwise regression model, and (c) partial least squares (PLS) model. Model performance indicators R^2 and root mean square error (RMSE) for each site are presented. LM, linear regression model.

TABLE 6 Pearson correlation coefficient (R^2) between UAV-derived traits (VIs and geometric traits) and total aboveground biomass across three field trials (Allora22, Gatton22, and Gatton23).

Trait	Early-canopy development	Mid-canopy development	Late-canopy development
NDRE	0.44	0.71	0.31
NDVI	0.71	0.08	0.4
OSAVI	0.66	0.62	0.33
Thermal	−0.72	−0.29	0
Coverage	0.9[a]	0.7	0.41[a]
Height	0.35	0.73[a]	0.27
Volume	0.77	0.54	0.32

Abbreviations: LM, linear regression model; NDRE, normalized difference red edge; NDVI, normalized difference vegetation index; OSAVI, optimized soil-adjusted vegetation index; UAV, unmanned aerial vehicle; VI, vegetative index.

[a]UAV trait with the strongest relationship with trait and used in LM approach.

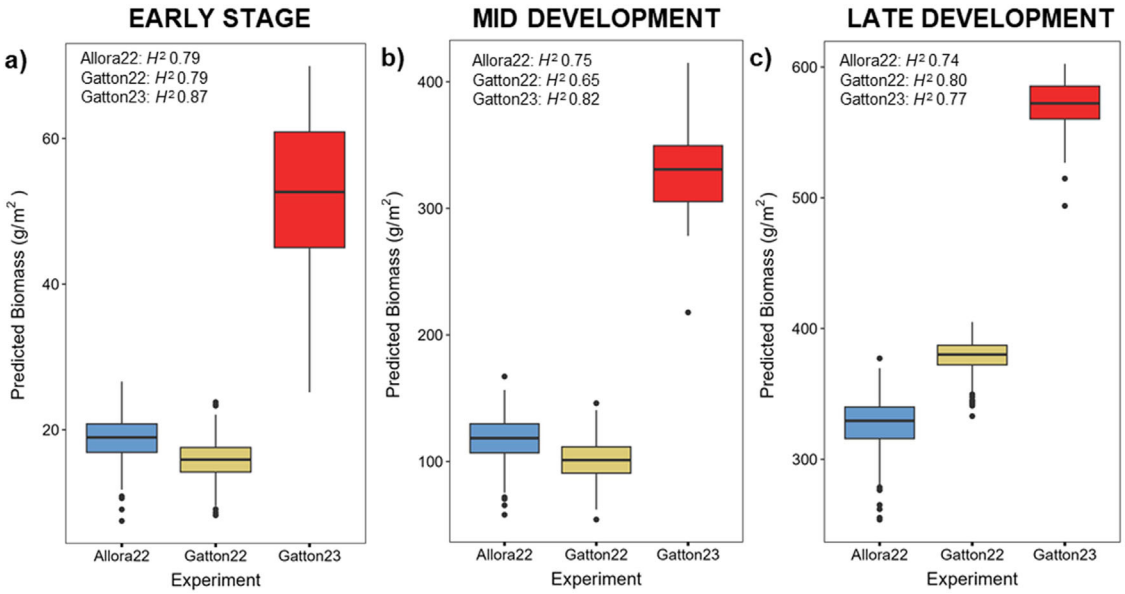

FIGURE 5 Best linear unbiased estimates (BLUEs) for aboveground biomass predicted across three key development stages captured across the mungbean diversity panel at Allora22 (blue), Gatton22 (yellow), and Gatton23 (red). (a) Early-, (b) mid-, and (c) late-canopy development. Broad-sense heritability was estimated for each development stage at each site and presented.

performed best (R^2 0.69, RMSE 0.10) (Figure 6c) with thermal being the largest contributor to the model, followed by NDRE, volume, height, OSAVI, and NDVI (Figure S4). The next highest performing approach was the SWR model using coverage, height, and thermal as predictors (R^2 0.67, RMSE 0.10) and LM using thermal (R^2 0.62, RMSE 0.11) (Figure 6a,b).

The best-performing model was used to predict g_{sw} across the entire field trial, and BLUEs were estimated for each genotype. Using this approach, significant phenotypic variation was observed at each location as well as variation across locations (Figure 6d). Gatton22 had overall higher g_{sw} values compared to Allora22 (0.25–0.52 and 0.05–0.19, respectively). The predicted values across both trials also had high broad-sense heritability (Allora22: 0.49, Gatton22: 0.87). Comparing Crystal to the other NAM parents, it was noted that Crystal had moderate stomatal conductance values across Allora22 and Gatton22 (0.1–0.38 mmol m^{-2} s^{-1}, respectively) (Table S5). In Allora22, Satin and AGG 325975 had the highest values (0.12 and 0.12 mmol m^{-2} s^{-1}, respectively), whereas in Gatton22, AGG 325975, AGG 325954, AGG 325959, and AGG 325958 had the highest stomatal conductance (0.46–0.5 mmol m^{-2} s^{-1}).

5 | DISCUSSION

In this study, four UAV-derived VIs and three geometric traits were evaluated, providing an efficient and non-destructive tool to phenotype important agronomic and physiological

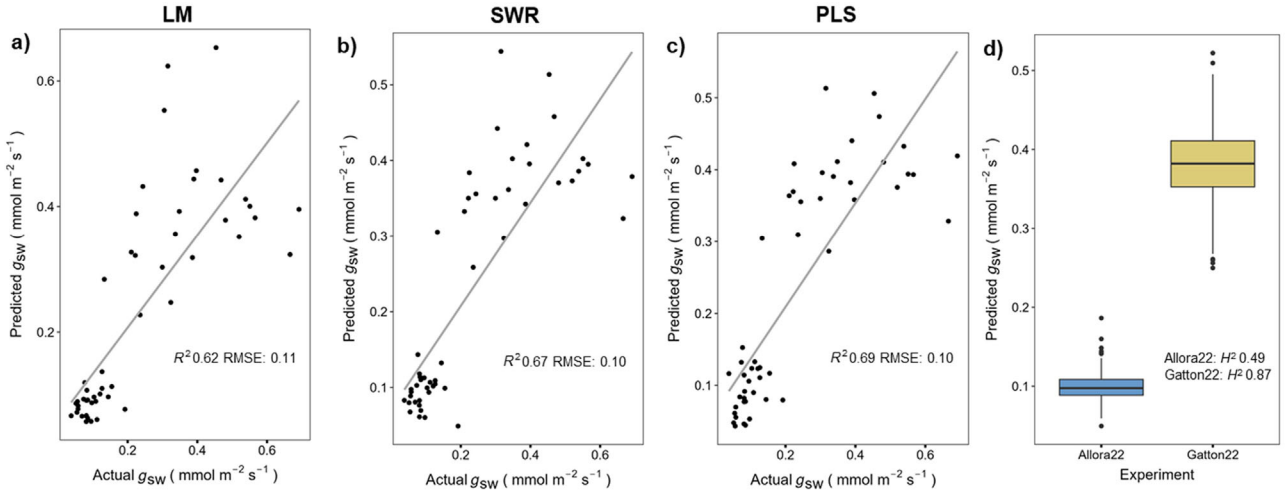

FIGURE 6 Stomatal conductance estimation results from two trials (Allora22 and Gatton22) determined at the reproductive stage using prediction models developed from vegetative indices (VIs) and geometric traits. (a) linear regression model (LM), (b) stepwise regression model (SWR), and (c) partial least squares (PLS) model, (d) best unbiased linear estimates (BLUEs) of stomatal conductance predictions across all plots in Allora22 and Gatton22. Model performance criteria (R^2 and root mean square error [RMSE]) are presented for each model. LM, linear regression model.

TABLE 7 Pearson correlation coefficient (R^2) between UAV-derived traits (VIs and geometric traits) and stomatal conductance across two field trials (Allora22 and Gatton22).

Trait	g_{sw}
NDRE	0.74
NDVI	0.5
OSAVI	0.47
Thermal	0.79[a]
Coverage	0.61
Height	0.51
Volume	0.48

Abbreviations: LM, linear regression model; NDRE, normalized difference red edge; NDVI, normalized difference vegetation index; OSAVI, optimized soil-adjusted vegetation index; UAV, unmanned aerial vehicle; VI, vegetative index.

[a]UAV trait with the strongest relationship and used in LM approach.

traits such as early vigor, aboveground biomass, and stomatal conductance. Statistical approaches were used to predict each trait across a large and diverse mungbean pre-breeding population and three field trials. Compared to traditional field-based phenotyping methods, which can be time-consuming and limiting in the number of genotypes that can be evaluated, UAV phenotyping platforms can collect data for a large-scale field trial in a fraction of the time. In the case of this study, flying a trial over 1.5 ha in size took only 25 min compared to the 2–3 h to collect visual vigor scores and stomatal conductance measurements as well as over 6 days to collect, dry, and weigh biomass samples. This efficiency makes UAV phenotyping a highly scalable solution, particularly for larger breeding programs, whereby collecting data across multiple hectares and locations becomes significantly faster compared to traditional ground-based measurements. Overall, the data derived from the multispectral sensor could be used to accurately predict the traits of interest, demonstrating the effectiveness of the platform to predict different types of visual, functional, and physiological traits typically captured in breeding and pre-breeding activities.

5.1 | UAV-derived traits can be used to enhance the accuracy and repeatability of phenotyping early vigor

A range of important agronomic traits are traditionally captured using visual scoring. This scoring system, while subjective, is the established standard in breeding programs due to its rapid and cost-effective nature, allowing breeders to quickly assess large numbers of breeding lines across multiple environments. However, due to the categorical nature of visual scoring, human bias can be introduced, and the resolution of data can be limited. Using UAV-derived traits, we have demonstrated that the use of coverage as a proxy trait offers a valuable, timely, and cost-effective solution to screening early vigor in the field. Predicting vigor using coverage improved heritability across all environments compared to the traditional visual scoring approach, which is critical for selection in breeding programs. While substantial differences in phenotypic values were observed between environments, the high heritability estimates reflect the consistency of genetic effects within each environment. Such variation in

heritability across environments is often seen in multiple field experiments (Brunner et al., 2024), and indicates that while environmental conditions strongly influence phenotypic values, the UAV-based measurements effectively capture the genetic differences between lines within each environment. Further, weak correlations were observed between VIs and vigor scores, which suggests that visual scores are not always a reliable ground truth. Previous studies in field pea have also demonstrated that VIs can be an effective proxy of early vigor under both controlled and field conditions (Nguyen et al., 2018; Tefera et al., 2022). In this study, to quantify the value of UAV-based phenotyping for early vigor, we compared the use of coverage as a proxy and traditional visual scoring (Figure 3). The negative correlation between drone-derived coverage and ground-based vigor scores was expected, as plots with higher coverage naturally correspond to lower numerical vigor scores (where 1 represents the most vigorous plants). This revealed that genotypes assigned the same categorical score showed a high degree of variation in coverage which suggests that coverage may be a more reliable measure of early vigor than traditional visual scoring in mungbean. Our analyses also identified genotypes with higher vigor compared to Crystal. These genotypes may be worthy of further investigation as enhancing early vigor is a key trait in mungbean breeding programs to improve weed competitiveness (B. S. Chauhan & Gill, 2014). Vigor was also noted to vary across environments with higher vigor values in Gatton22 compared to Gatton23 and Allora22. The UAV-based phenotyping platform therefore provides the necessary data to undertake genotype × environment analyses and begin to understand the effect of the environment on early vigor. The higher resolution resulting from utilizing the UAV approach may offer the potential to accurately identify genotypes of interest that are performing higher overall across a large population as well as the overall performance of genotypes across environments. Using more reliable phenotyping approaches to screen for early vigor will likely increase the accuracy of quantitative trait locus (QTL) mapping studies aiming to unravel the genetic components of early vigor in mungbean.

5.2 | Aboveground biomass can be predicted across a high spatiotemporal scale

Aboveground biomass is a functional plant development trait that is a crucial determinant of yield due to its function in light interception, assimilate supply, and adaptability to environmental responses (e.g., Turner et al., 2001). Rapidly screening for aboveground biomass non-destructively enables data capture at a larger spatial and temporal scale and provides insight into detailed canopy traits that cannot be captured on the ground. Previous mungbean studies evaluating canopy dynamics have been limited to a small number of genotypes, highlighting a major phenotyping gap (Geetika, Collins et al., 2022; Kaur et al., 2015; Xiong et al., 2023). This study was able to develop biomass prediction models using a diverse mungbean population with substantial variation in canopy architecture, providing new insight into mungbean canopy development. These models could therefore be valuable in understanding how commercial cultivars, such as Crystal, perform across different production environments. Additionally, they could enable the investigation of new genetics available in breeding programs or diverse genebank accessions that may harbor novel canopy traits. From our results, it was observed that there were several genotypes that accumulated higher and lower biomass at different stages compared to Crystal, which may be of value in different environments or farming systems. For example, genotypes AGG 325966 and Berken had higher biomass compared to Crystal at the early-canopy development stage. In optimal conditions where water is not limiting, higher biomass at this stage may enhance light capture and radiation use efficiency leading to increased productivity. Conversely, in water-limited environments, there may be potential trade-offs with water uptake that need to be considered as a vigorous high-biomass genotype could exhaust soil water supply and increase the risk of drought stress later in the season.

A key finding from this research is the need to apply different prediction model approaches and UAV-derived traits at different time points. At the early-canopy development stage, a simple LM with canopy coverage works well to predict biomass. This was unsurprising as mungbean has previously been determined to have a horizontal canopy architecture (radiation extinction coefficient 0.68) (Geetika, Collins et al., 2022), which demonstrates that the UAV is able to capture the entire canopy from above at this stage. The importance of coverage at the vegetative stage in mungbean was also identified by Xiong et al. (2023), although this approach did not result in strong correlations post-flowering using fractional vegetative cover and VIs alone. Our research reinforces the need for more complex modeling approaches to predict biomass during mid- and late-canopy development stages, which is when post-flowering, pod development, and senescence occur. During later canopy development stages, the incorporation of geometric traits such as height and coverage, as well as VIs linked to senescence such as NDRE, significantly improves the model accuracy (Varela et al., 2021) as the canopy is entirely closed and biomass cannot be determined accurately from a single VI captured above the canopy. The incorporation of geometric traits to predict biomass has also been undertaken in barley (Bendig et al., 2015) and wheat (Yue et al., 2017). While utilizing different prediction models and UAV-derived traits at different canopy development stages is complex as a result of changes in physiology, this approach ensures biomass can be accurately predicted across all canopy development stages in mungbean. There are

opportunities to further improve the accuracy of biomass prediction in late-canopy development stages. Future studies may utilize alternative modeling techniques or engineering approaches to evaluate potential improvements to prediction accuracy to capture the complexity of aboveground biomass during reproductive growth stages.

Modeling biomass across key developmental stages provides the fundamental components required to dissect mungbean canopy dynamic traits, such as rate and magnitude of canopy development and senescence through a longitudinal modeling approach. This type of longitudinal modeling has been undertaken to evaluate stay green traits in sorghum, barley, and wheat using the single vegetation index NDVI (Brunner et al., 2024; Liedtke et al., 2020; Thapa et al., 2019). A recent study applied a new two-stage longitudinal modeling strategy that first fit a spatial model to correct the data at each timepoint and then fit a p-spline across all datapoints to extract key growth curve parameters from two field trials conducted in different phenotyping platforms (Pérez-Valencia et al., 2022). Additionally, exploring these canopy dynamic traits in the context of abiotic and biotic stresses offers the opportunity to identify new physiological and genetic mechanisms that infer adaptation that could be incorporated into breeding programs.

5.3 | Beyond the breeders' eye: Utilizing the UAV platform to assess physiological traits

In this study, we have demonstrated the capacity of UAV-derived traits in exploring stomatal conductance, which is a complex physiological trait that cannot be captured directly by visual scores. Current methods used to determine stomatal conductance, such as porometers, are relatively rapid. However, as stomatal conductance fluctuates quickly over the course of the day and with varying environmental conditions, there are substantial challenges in capturing a large number of genotypes and accurately comparing output. Comparatively, using a UAV phenotyping platform across over 600 plots (391–410 genotypes) took only 20 min. There is now a growing number of studies that aim to link UAV-derived traits and g_{sw} on other major crops. For example, a 2022 study conducted using 91 tomato genotypes under well-watered and water-deficit treatments determined that NDVI had a significant positive relationship with g_{sw} as well as total assimilation rate (Fullana-Pericàs et al., 2022). Another study in maize utilized random forest prediction models with several VIs and determined that primarily thermal infrared regions and a number of near-infrared and red-based VIs significantly contributed to g_{sw} prediction during vegetative growth, while later development (reproductive stages) relied mostly on near-infrared and red-based VIs (Brewer et al., 2022). This research supports the findings observed in this study where the thermal band and NDRE (uses both near infrared and red edge bands) were determined to be significant contributors to the highest performing prediction model for $g_{sw,}$ as well as volume, height, OSAVI, and NDVI, which contribute only a small amount. The incorporation of thermal is most likely linked to the relationship observed between canopy temperature and g_{sw}, whereby as the stomata close, the internal temperature of the leaf increases due to the lack of transpiration occurring to cool the canopy. Whereas the contribution of NDRE to the model is likely a result of the indices relationship with the amount of chlorophyll in the plant and the amount of photosynthetically active leaf area present in the plot, which highlights the causal relationship that is typically found between chlorophyll content in the leaves and stomatal aperture (i.e., less chlorophyll leads to reduced stomatal aperture) (Matsumoto et al., 2005). Therefore, as the plant transitions from vegetative to reproductive development, the change in chlorophyll content may be a more significant driver rather than actual changes in stomatal aperture per se. We acknowledge that it is difficult to develop "generic" prediction models of traits that work in all situations and recommend that in using UAV for large-scale trials, researchers can benefit from using the UAV to scan the entire trial (perhaps thousands of plots) while taking additional phenotypic data or scores on a limited subset of plots (for instance, 30–50). Models developed from these subsets can then be applied to the UAV multispectral results as proposed by Hu et al. (2018) and Baret et al. (2018) and have been referred to as a "real-time calibration" approach.

This study successfully detected genetic variation for g_{sw} from UAV spectral data, which may be further explored for crop improvement to match specific production environments. Our findings highlight that there may be potential to increase the stomatal conductance of commercial cultivar Crystal which was found to be more conservative in its stomatal conductance across environments compared to a range of diverse accessions such as AGG 325958 and AGG 325975. Therefore, the water use efficiency of accessions can now be evaluated in irrigated environments as they may be able to support higher g_{sw} or within rainfed environments where periods of water deficit may be experienced and higher water use efficiency is beneficial. Genetic mechanisms underpinning stomatal conductance may also be explored which is not easily undertaken using traditional approaches. Nevertheless, to further enhance the model, additional data may be collected to accurately predict g_{sw} in a wider range of environment types.

6 | CONCLUSION

The phenotyping bottleneck in mungbean has constrained the identification of important traits and associated genetic mechanisms required to rapidly and efficiently improve mungbean

productivity. We demonstrate the potential of using UAV-based phenotyping platforms to screen and predict several different agronomic traits of a diverse mungbean population across multiple field trials that are traditionally captured visually (early vigor), using specialized physiological tools (stomatal conductance), or destructively (aboveground biomass). For all traits, the important role of adjusting prediction model approaches depending on trait type (categorical, physiological, and functional) and developmental stage at the time of capture was highlighted. The variation in prediction accuracy across growth stages reflects multiple underlying biological factors including canopy closure and the initiation of complex physiological processes (e.g., increased branching and pod senescence). Further exploration of how these traits can be more accurately captured using other indices or developing new indices may be explored in future studies to improve prediction accuracy for later growth stages. Despite these challenges, robust phenotyping methods for early vigor, stomatal conductance, and biomass have now been established for mungbean and applied to explore genetic variation at a high resolution and spatial scale. Further studies using these models to undertake genotype × environment analyses, longitudinal analyses to extract dynamic traits as well as genetic analyses are suggested to explore the potential of using this platform to further accelerate mungbean improvement.

AUTHOR CONTRIBUTIONS

Shanice Van Haeften: Conceptualization; data curation; formal analysis; writing—original draft; writing—review and editing. **Daniel Smith**: Methodology; writing—review and editing. **Hannah Robinson**: Supervision; writing—review and editing. **Caitlin Dudley**: Data curation; writing—review and editing. **Yichen Kang**: Writing—review and editing. **Colin A. Douglas**: Supervision; writing—review and editing. **Lee T. Hickey**: Conceptualization; writing—review and editing. **Scott Chapman**: Methodology; writing—review and editing. **Andries Potgieter**: Methodology; supervision; writing—review and editing. **Millicent R. Smith**: Conceptualization; funding acquisition; supervision; writing—review and editing.

ACKNOWLEDGMENTS

This research was funded by Grains Research and Development Corporation (GRDC; UOQ2101-003RSX) and supported by the International Mungbean Improvement Network (ACIAR; CIM2014/079). Shanice Van Haeften is the recipient of an Australian Government Research Training (RTP) scholarship. We acknowledge Airborne Insights for capturing the UAV flights throughout the Allora22 trial and GRDC project UOQ2003-011RTX, which supported research of Daniel Smith in developing the image processing pipelines and the baseline models for biomass prediction. We also acknowledge the technical and casual staff, particularly Sarah van der Meer, for their assistance with sample collection in the field.

Open access publishing facilitated by The University of Queensland, as part of the Wiley - The University of Queensland agreement via the Council of Australian University Librarians.

CONFLICT OF INTEREST STATEMENT

The authors declare no conflicts of interest.

DATA AVAILABILITY STATEMENT

This dataset is available at UQ eSpace: https://doi.org/10.48610/20cffed.

ORCID

Shanice Van Haeften https://orcid.org/0000-0003-0412-3457
Daniel Smith https://orcid.org/0000-0002-5867-9613
Hannah Robinson https://orcid.org/0000-0002-8303-8076
Caitlin Dudley https://orcid.org/0000-0001-5297-7487
Yichen Kang https://orcid.org/0000-0002-3613-7426
Lee T. Hickey https://orcid.org/0000-0001-6909-7101
Andries Potgieter https://orcid.org/0000-0002-1671-8266
Scott Chapman https://orcid.org/0000-0003-4732-8452
Millicent R. Smith https://orcid.org/0000-0003-1749-2884

REFERENCES

ABARES. (2020). *Australian crop report*. Australian Bureau of Agricultural and Resource Economics and Sciences. https://doi.org/10.25814/5e3a014fa7e2d

Aparicio, N., Villegas, D., Casadesus, J., Araus, J. L., & Royo, C. (2000). Spectral vegetation indices as nondestructive tools for determining durum wheat yield. *Agronomy Journal*, *92*(1), 83–91. https://doi.org/10.2134/agronj2000.92183x

Australian Centre for International Agricultural Research (ACIAR). (2022). Establishing the international mungbean improvement network *(CIM/2014/079)*. ACIAR. https://www.aciar.gov.au/project/cim-2014-079

Barboza, T. O. C., Ardigueri, M., Souza, G. F. C., Ferraz, M. A. J., Gaudencio, J. R. F., & Santos, A. F. D. (2023). Performance of vegetation indices to estimate green biomass accumulation in common bean. *AgriEngineering*, *5*(2), 840–854. https://doi.org/10.3390/agriengineering5020052

Baret, F., Madec, S., Irfan, K., Lopez, J., Comar, A., Hemmerlé, M., Dutartre, D., Praud, S., & Tixier, M. H. (2018). Leaf-rolling in maize crops: From leaf scoring to canopy-level measurements for phenotyping. *Journal of Experimental Botany*, *69*(10), 2705–2716. https://doi.org/10.1093/jxb/ery071

Bendig, J., Yu, K., Aasen, H., Bolten, A., Bennertz, S., Broscheit, J., Gnyp, M. L., & Bareth, G. (2015). Combining UAV-based plant height from crop surface models, visible, and near infrared vegetation indices for biomass monitoring in barley. *International Journal of Applied Earth Observation and Geoinformation*, *39*, 79–87. https://doi.org/10.1016/j.jag.2015.02.012

Bertholdsson, N. O. (2005). Early vigor and allelopathy–two useful traits for enhanced barley and wheat competitiveness against weeds. *Weed*

Research, *45*(2), 94–102. https://doi.org/10.1111/j.1365-3180.2004.00442.x

Bertolino, L. T., Caine, R. S., & Gray, J. E. (2019). Impact of stomatal density and morphology on water-use efficiency in a changing world. *Frontiers in Plant Science*, *10*, Article 225. https://doi.org/10.3389/fpls.2019.00225

Borra-Serrano, I., De Swaef, T., Quataert, P., Aper, J., Saleem, A., Saeys, W., Somers, B., Roldán-Ruiz, I., & Lootens, P. (2020). Closing the phenotyping gap: High resolution UAV time series for soybean growth analysis provides objective data from field trials. *Remote Sensing*, *12*(10), 1644. https://doi.org/10.3390/rs12101644

Brewer, K., Clulow, A., Sibanda, M., Gokool, S., Odindi, J., Mutanga, O., Naiken, V., Chimonyo, V. G. P., & Mabhaudhi, T. (2022). Estimation of maize foliar temperature and stomatal conductance as indicators of water stress based on optical and thermal imagery acquired using an unmanned aerial vehicle (UAV) platform. *Drones*, *6*(7), 169. https://doi.org/10.3390/drones6070169

Brunner, S. M., Dinglasan, E., Baraibar, S., Alahmad, S., Katsikis, C., van der Meer, S., Godoy, J., Moody, D., Smith, M., Hickey, L., & Robinson, H. (2024). Characterizing stay-green in barley across diverse environments: Unveiling novel haplotypes. *Theoretical and Applied Genetics*, *137*(6), Article 120. https://doi.org/10.1007/s00122-024-04612-1

Butler, D. G., Cullis, B. R., Gilmour, A. R., & Gogel, B. J. (2009). *ASReml-R reference manual*. The State of Queensland, Department of Primary Industries and Fisheries.

Chapman, S. C., Merz, T., Chan, A., Jackway, P., Hrabar, S., Dreccer, M. F., Holland, E., Zheng, B., Ling, J. T., & Jimenez-Berni, J. (2014). Pheno-copter: A low-altitude, autonomous remote-sensing robotic helicopter for high-throughput field-based phenotyping. *Agronomy*, *4*(2), 279–301. https://doi.org/10.3390/agronomy4020279

Chauhan, B. S., & Gill, G. S. (2014). Ecologically based weed management strategies. In B. S., Chauhan & G. Mahajan (Eds.), *Recent advances in weed management* (pp. 1–11). Springer. https://doi.org/10.1007/978-1-4939-1019-9_1

Chauhan, Y. S., & Williams, R. (2018). Physiological and agronomic strategies to increase mungbean yield in climatically variable environments of northern Australia. *Agronomy*, *8*(6), Article 83. https://doi.org/10.3390/agronomy8060083

Colgrave, M. L., Dominik, S., Tobin, A. B., Stockmann, R., Simon, C., Howitt, C. A., Belobrajdic, D. P., Paull, C., & Vanhercke, T. (2021). Perspectives on future protein production. *Journal of Agricultural and Food Chemistry*, *69*(50), 15076–15083. https://doi.org/10.1021/acs.jafc.1c05989

Collins, M., Anderson, B., & Bell, L. (2019). *Yield gaps in mungbean crops across the northern grains region*. Grains Research and Development Corporation. https://grdc.com.au/resources-and-publications/grdc-update-papers/tab-content/grdc-update-papers/2019/08/yield-gaps-in-mungbean-crops-across-the-northern-grains-region

Conaty, W. C., Mahan, J. R., Neilsen, J. E., Tan, D. K., Yeates, S. J., & Sutton, B. G. (2015). The relationship between cotton canopy temperature and yield, fibre quality and water-use efficiency. *Field Crops Research*, *183*, 329–341. https://doi.org/10.1016/j.fcr.2015.08.010

Condon, A. G., Richards, R. A., Rebetzke, G. J., & Farquhar, G. D. (2004). Breeding for high water-use efficiency. *Journal of Experimental Botany*, *55*(407), 2447–2460. https://doi.org/10.1093/jxb/erh277

Crusiol, L., Nanni, M., Herrig Furlanetto, R., Sibaldelli, R., Cezar, E., Mertz-Henning, L., Nepomuceno, A. L., Neumaier, N., Ronato, J., & Farias, J. (2019). UAV-based thermal imaging in the assessment of water status of soybean plants. *International Journal of Remote Sensing*, *41*(9), 3243–3265. https://doi.org/10.1080/01431161.2019.1673914

Cullis, B. R., Smith, A. B., Cocks, N. A., & Butler, D. G. (2020). The design of early-stage plant breeding trials using genetic relatedness. *Journal of Agricultural, Biological and Environmental Statistics*, *25*(4), 553–578. https://doi.org/10.1007/s13253-020-00403-5

Cullis, B. R., Smith, A. B., & Coombes, N. E. (2006). On the design of early generation variety trials with correlated data. *Journal of Agricultural, Biological, and Environmental statistics*, *11*, 381–393. https://doi.org/10.1198/108571106x154443

Das, S., Massey-Reed, S. R., Mahuika, J., Watson, J., Cordova, C., Otto, L., Zhao, Y., Chapman, S., George-Jaeggli, B., Jordan, D., Hammer, G. L., & Potgieter, A. B. (2022). A high-throughput phenotyping pipeline for rapid evaluation of morphological and physiological crop traits across large fields. In *IGARSS 2022—2022 IEEE international geoscience and remote sensing symposium* (pp. 7783–7786). IEEE. https://doi.org/10.1109/IGARSS46834.2022.9884530

Fitzgerald, G. J., Rodriguez, D., Christensen, L. K., Belford, R., Sadras, V. O., & Clarke, T. R. (2006). Spectral and thermal sensing for nitrogen and water status in rainfed and irrigated wheat environments. *Precision Agriculture*, *7*, 233–248. https://doi.org/10.1007/s11119-006-9011-z

Fullana-Pericàs, M., Conesa, M. À., Gago, J., Ribas-Carbó, M., & Galmés, J. (2022). High-throughput phenotyping of a large tomato collection under water deficit: Combining UAVs' remote sensing with conventional leaf-level physiologic and agronomic measurements. *Agricultural Water Management*, *260*, 107283. https://doi.org/10.1016/j.agwat.2021.107283

Furbank, R. T., Jimenez-Berni, J. A., George-Jaeggli, B., Potgieter, A. B., & Deery, D. M. (2019). Field crop phenomics: enabling breeding for radiation use efficiency and biomass in cereal crops. *New Phytologist*, *223*(4), 1714–1727. https://doi.org/10.1111/nph.15817

Gano, B., Dembele, J. S. B., Ndour, A., Luquet, D., Beurier, G., Diouf, D., & Audebert, A. (2021). Using UAV borne, multi-spectral imaging for the field phenotyping of shoot biomass, leaf area index and height of West African sorghum varieties under two contrasted water conditions. *Agronomy*, *11*(5), 850. https://doi.org/10.3390/agronomy11050850

Geetika, G., Collins, M., Singh, V., Hammer, G., Mellor, V., Smith, M., & Rachaputi, R. C. (2022). Canopy and reproductive development in mungbean (*Vigna radiata*). *Crop & Pasture Science*, *73*(10), 1142–1155. https://doi.org/10.1071/CP21209

Geetika, G., Hammer, G., Smith, M., Singh, V., Collins, M., Mellor, V., Wenham, K., & Rachaputi, R. C. (2022). Quantifying physiological determinants of potential yield in mungbean (*Vigna radiata* (L.) Wilczek). *Field Crops Research*, *287*, 108648. https://doi.org/10.1016/j.fcr.2022.108648

Gentry, J. (2010). *Mungbean management guide* (2nd ed.). Department of Employment, Economic Development and Innovation. https://era.daf.qld.gov.au/id/eprint/7070/1/mung-manual2010-LR.pdf

Gitelson, A. A., Kaufman, Y. J., & Merzlyak, M. N. (1996). Use of a green channel in remote sensing of global vegetation from EOS-MODIS. *Remote Sensing of Environment*, *58*(3), 289–298. https://doi.org/10.1016/S0034-4257(96)00072-7

Grains Research and Development Corporation (GRDC). (2017). *Mungbeans northern region—GrowNotes*. GRDC. https://grdc.com.au/resources-and-publications/grownotes/crop-agronomy/grownotesmungbeansnorthern

Hassan, M. A., Yang, M., Fu, L., Rasheed, A., Zheng, B., Xia, X., Xiao, Y., & He, Z. (2019). Accuracy assessment of plant height using an unmanned aerial vehicle for quantitative genomic analysis in bread wheat. *Plant Methods*, *15*(1), Article 37. https://doi.org/10.1186/s13007-019-0419-7

Hassan, M. A., Yang, M., Rasheed, A., Jin, X., Xia, X., Xiao, Y., & He, Z. (2018). Time-series multispectral indices from unmanned aerial vehicle imagery reveal senescence rate in bread wheat. *Remote Sensing*, *10*(6), 809. https://doi.org/10.3390/rs10060809

Hatfield, J. L., & Prueger, J. H. (2010). Value of using different vegetative indices to quantify agricultural crop characteristics at different growth stages under varying management practices. *Remote Sensing*, *2*(2), 562–578. https://doi.org/10.3390/rs2020562

Hikosaka, K. (2005). Leaf canopy as a dynamic system: Ecophysiology and optimality in leaf turnover. *Annals of Botany*, *95*(3), 521–533. https://doi.org/10.1093/aob/mci050

Hu, P., Chapman, S. C., Wang, X., Potgieter, A., Duan, T., Jordan, D., Guo, Y., & Zheng, B. (2018). Estimation of plant height using a high throughput phenotyping platform based on unmanned aerial vehicle and self-calibration: Example for sorghum breeding. *European Journal of Agronomy*, *95*, 24–32. https://doi.org/10.1016/j.eja.2018.02.004

Huete, A., Didan, K., Miura, T., Rodriguez, E. P., Gao, X., & Ferreira, L. G. (2002). Overview of the radiometric and biophysical performance of the MODIS vegetation indices. *Remote Sensing of Environment*, *83*(1–2), 195–213. https://doi.org/10.1016/S0034-4257(02)00096-2

Kaur, R., Bains, T. S., Bindumadhava, H., & Nayyar, H. (2015). Responses of mungbean (*Vigna radiata* L.) genotypes to heat stress: Effects on reproductive biology, leaf function and yield traits. *Scientia Horticulturae*, *197*, 527–541. https://doi.org/10.1016/j.scienta.2015.10.015

Kim, S. K., Nair, R. M., Lee, J., & Lee, S.-H. (2015). Genomic resources in mungbean for future breeding programs. *Frontiers in Plant Science*, *6*. https://doi.org/10.3389/fpls.2015.00626

Kipp, S., Mistele, B., Baresel, P., & Schmidhalter, U. (2014). High-throughput phenotyping early plant vigour of winter wheat. *European Journal of Agronomy*, *52*, 271–278. https://doi.org/10.1016/j.eja.2013.08.009

Li, S., Ding, X., Kuang, Q., Ata-UI-Karim, S. T., Cheng, T., Liu, X., Tian, Y., Zhu, Y., Cao, W., & Cao, Q. (2018). Potential of UAV-based active sensing for monitoring rice leaf nitrogen status. *Frontiers in Plant Science*, *9*. https://doi.org/10.3389/fpls.2018.01834

Liedtke, J. D., Hunt, C. H., George-Jaeggli, B., Laws, K., Watson, J., Potgieter, A. B., Cruickshank, A., & Jordan, D. R. (2020). High-throughput phenotyping of dynamic canopy traits associated with stay-green in grain sorghum. *Plant Phenomics*, *2020*, Article 4635153. https://doi.org/10.34133/2020/4635153

Maimaitijiang, M., Sagan, V., Sidike, P., Maimaitiyiming, M., Hartling, S., Peterson, K. T., Maw, M. J. W., Shakoor, N., Mockler, T., & Fritschi, F. B. (2019). Vegetation index weighted canopy volume model (CVMVI) for soybean biomass estimation from unmanned aerial system-based RGB imagery. *ISPRS Journal of Photogrammetry and Remote Sensing*, *151*, 27–41. https://doi.org/10.1016/j.isprsjprs.2019.03.003

Malambo, L., Popescu, S. C., Murray, S. C., Putman, E., Pugh, N. A., Horne, D. W., Richardson, G., Sheridan, R., Rooney, W. L., Avant, R., Vidrine, M., McCutchen, B., Baltensperger, D., & Bishop, M. (2018). Multitemporal field-based plant height estimation using 3D point clouds generated from small unmanned aerial systems high-resolution imagery. *International Journal of Applied Earth Observation and Geoinformation*, *64*, 31–42. https://doi.org/10.1016/j.jag.2017.08.014

Matsumoto, K., Ohta, T., & Tanaka, T. (2005). Dependence of stomatal conductance on leaf chlorophyll concentration and meteorological variables. *Agricultural and Forest Meteorology*, *132*(1–2), 44–57. https://doi.org/10.1016/j.agrformet.2005.07.001

Nair, R., & Schreinemachers, P. (2020). Global status and economic importance of mungbean. In R., Nair, R., Schafleitner, & S. H., Lee (Eds.), *The mungbean genome* (pp. 1–8). Springer.

Nguyen, G. N., Norton, S. L., Rosewarne, G. M., James, L. E., & Slater, A. T. (2018). Automated phenotyping for early vigour of field pea seedlings in controlled environment by colour imaging technology. *PLoS ONE*, *13*(11), e0207788. https://doi.org/10.1371/journal.pone.0207788

Noble, T. (2017). *Development of the mungbean nested association mapping (NAM) resource* [Conference presentation abstract]. InterDrought V, Hyderabad, India.

Otsu, N. (1979). A threshold selection method from gray-level histograms. *IEEE Transactions on Systems, Man, and Cybernetics*, *9*(1), 62–66. https://doi.org/10.1109/TSMC.1979.4310076

Pasley, H., Wenham, K., Bell, L., Huth, N., Holzworth, D., Chaki, A., Gaydon, D., & Collins, M. (2023). APSIM next generation mungbean model: A tool for advancing mungbean production. *Field Crops Research*, *298*, 108955. https://doi.org/10.1016/j.fcr.2023.108955

Patriyawaty, N. R., Rachaputi, R. C., George, D., & Douglas, C. (2018). Genotypic variability for tolerance to high temperature stress at reproductive phase in mungbean [Vigna radiata (L.) Wilczek]. *Scientia Horticulturae*, *227*, 132–141. https://doi.org/10.1016/j.scienta.2017.09.017

Pérez-Valencia, D. M., Rodríguez-Álvarez, M. X., Boer, M. P., Kronenberg, L., Hund, A., Cabrera-Bosquet, L., Millet, E., & Eeuwijk, F. A. V. (2022). A two-stage approach for the spatio-temporal analysis of high-throughput phenotyping data. *Scientific Reports*, *12*(1), Article 3177. https://doi.org/10.1038/s41598-022-06935-9

Pieruschka, R., & Schurr, U. (2019). Plant phenotyping: Past, present, and future. *Plant Phenomics*, *2019*, Article 7507131. https://doi.org/10.34133/2019/7507131

Potgieter, A. B., Watson, J., George-Jaeggli, B., McLean, G., Eldridge, M., Chapman, S. C., Laws, K., Christopher, J., Chenu, K., Borrell, A., Hammer, G. R., & Jordan, D. J. (2018). The use of hyperspectral proximal sensing for phenotyping of plant breeding trials. In *Fundamentals, sensor systems, spectral libraries, and data mining for vegetation* (pp. 127–147) edited by Prasad S. Thenkabail, John G. Lyon and Alfredo Huete. CRC Press Taylor and Francis Group.

Rachaputi, R. C. N., Sands, D., McKenzie, K., Agius, P., Lehane, J., & Seyoum, S. (2019). Eco-physiological drivers influencing mungbean [Vigna radiata (L.) Wilczek] productivity in subtropical Australia. *Field Crops Research*, *238*, 74–81. https://doi.org/10.1016/j.fcr.2019.04.023

Rebetzke, G. J., & Richards, R. A. (1999). Genetic improvement of early vigour in wheat. *Australian Journal of Agricultural Research*, *50*(3), 291–302. https://doi.org/10.1071/A98125

Robles-Zazueta, C. A., Molero, G., Pinto, F., Foulkes, M. J., Reynolds, M. P., & Murchie, E. H. (2021). Field-based remote sensing models predict radiation use efficiency in wheat. *Journal of Experimental Botany*, *72*(10), 3756–3773. https://doi.org/10.1093/jxb/erab115

Rondeaux, G., Steven, M., & Baret, F. (1996). Optimization of soil-adjusted vegetation indices. *Remote Sensing of Environment*, *55*(2), 95–107. https://doi.org/10.1016/0034-4257(95)00186-7

Rouse, J. W., Haas, R. H., Schell, J. A., & Deering, D. W. (1974). Monitoring vegetation systems in the Great Plains with ERTS. *NASA Special Publication*, *351*(1), 309.

Sandhu, K., & Singh, A. (2020). Strategies for the utilization of the USDA mung bean germplasm collection for breeding outcomes. *Crop Science*, *61*(1), 422–442. https://doi.org/10.1002/csc2.20322

Selvaraj, M. G., Valderrama, M., Guzman, D., Valencia, M., Ruiz, H., & Acharjee, A. (2020). Machine learning for high-throughput field phenotyping and image processing provides insight into the association of above and below-ground traits in cassava (*Manihot esculenta* Crantz). *Plant Methods*, *16*, Article 87. https://doi.org/10.1186/s13007-020-00625-1

Smith, D. T., Potgieter, A. B., & Chapman, S. C. (2021). Scaling up high-throughput phenotyping for abiotic stress selection in the field. *Theoretical and Applied Genetics*, *134*, 1845–186. https://doi.org/10.1007/s00122-021-03864-5

Smith, D. T., Chen, Q., Massey-Reed, S. R., Potgieter, A. B., & Chapman, S. C. (2024). Prediction accuracy and repeatability of UAV based biomass estimation in wheat variety trials as affected by variable type, modelling strategy and sampling location. *Plant Methods*, *20*(1), Article 129. https://doi.org/10.1186/s13007-024-01236-w

Smith, M. R., Rao, I. M., & Merchant, A. (2018). Source-sink relationships in crop plants and their influence on yield development and nutritional quality. *Frontiers in Plant Science*, *9*, Article 1889. https://doi.org/10.3389/fpls.2018.01889

Sulik, J. J., & Long, D. S. (2020). Automated detection of phenological transitions for yellow flowering Xiong plants such as *Brassica* oilseeds. *Agrosystems, Geosciences & Environment*, *3*(1), e20125. https://doi.org/10.1002/agg2.20125

Tefera, A. T., Banerjee, B. P., Pandey, B. R., James, L., Puri, R. R., Cooray, O., Marsh, J., Richard, M., Kant, S., Fitzgerald, G. J., & Rosewarne, G. M. (2022). Estimating early season growth and biomass of field pea for selection of divergent ideotypes using proximal sensing. *Field Crops Research*, *277*, 108407. https://doi.org/10.1016/j.fcr.2021.108407

Thapa, S., Rudd, J. C., Xue, Q., Bhandari, M., Reddy, S. K., Jessup, K. E., Shuyu, L., Devkota, R. N., Baker, J., & Baker, S. (2019). Use of NDVI for characterizing winter wheat response to water stress in a semi-arid environment. *Journal of Crop Improvement*, *33*(5), 633–648. https://doi.org/10.1080/15427528.2019.1648348

Thompson, C. G., Kim, R. S., Aloe, A. M., & Becker, B. J. (2017). Extracting the variance inflation factor and other multicollinearity diagnostics from typical regression results. *Basic and Applied Social Psychology*, *39*(2), 81–90. https://doi.org/10.1080/01973533.2016.1277529

Tunca, E., Köksal, E. S., & Taner, S. Ç. (2023). Calibrating UAV thermal sensors using machine learning methods for improved accuracy in agricultural applications. *Infrared Physics & Technology*, *133*, 104804. https://doi.org/10.1016/j.infrared.2023.104804

Turner, N. C., Wright, G. C., & Siddique, K. H. M. (2001). Adaptation of grain legumes (pulses) to water-limited environments. *Advances in Agronomy*, *71*, 193–231. https://doi.org/10.1016/s0065-2113(01)71015-2

Van Haeften, S., Dudley, C., Kang, Y., Smith, D., Nair, R. M., Douglas, C. A., Potgieter, A., Robinson, H., Hickey, L. T., & Smith, M. R. (2023). Building a better mungbean: Breeding for reproductive resilience in a changing climate. *Food and Energy Security*, *12*, e467. https://doi.org/10.1002/fes3.467

Varela, S., Pederson, T., Bernacchi, C. J., & Leakey, A. D. (2021). Understanding growth dynamics and yield prediction of sorghum using high temporal resolution UAV imagery time series and machine learning. *Remote Sensing*, *13*(9), 1763. https://doi.org/10.3390/rs13091763

Vina, A., Gitelson, A. A., Rundquist, D. C., Keydan, G., Leavitt, B., & Schepers, J. (2004). Monitoring maize (*Zea mays* L.) phenology with remote sensing. *Agronomy Journal*, *96*(4), 1139–1147. https://doi.org/10.2134/agronj2004.1139

Wang, D., Li, R., Zhu, B., Liu, T., Sun, C., & Guo, W. (2022). Estimation of wheat plant height and biomass by combining UAV imagery and elevation data. *Agriculture*, *13*(1), 9. https://doi.org/10.3390/agriculture13010009

Woebbecke, D. M., Meyer, G. E., Von Bargen, K., & Mortensen, D. A. (1995). Color indices for weed identification under various soil, residue, and lighting conditions. *Transactions of the ASAE*, *38*(1), 259–269. https://doi.org/10.13031/2013.27838

Xiong, Y., Chiau, L. M. R., Wenham, K., Collins, M., & Chapman, S. C. (2023). Utilisation of unmanned aerial vehicle imagery to assess growth parameters in mungbean (*Vigna radiata* (L.) Wilczek). *Crop & Pasture Science*, *75*(1), CP22335. https://doi.org/10.1071/CP22335

Yamashita, T., Yamashita, K., & Kamimura, R. (2007). A stepwise AIC method for variable selection in linear regression. *Communications in Statistics—Theory and Methods*, *36*(13), 2395–2403. https://doi.org/10.1080/03610920701215639

Yue, J., Yang, G., Li, C., Li, Z., Wang, Y., Feng, H., & Xu, B. (2017). Estimation of winter wheat above-ground biomass using unmanned aerial vehicle-based snapshot hyperspectral sensor and crop height improved models. *Remote Sensing*, *9*(7), 708. https://doi.org/10.3390/rs9070708

Zhi, X., Massey-Reed, S. R., Wu, A., Potgieter, A., Borrell, A., Hunt, C., Chapman, S., Hammer, G., & George-Jaeggli, B. (2022). Estimating photosynthetic attributes from high-throughput canopy hyperspectral sensing in sorghum. *Plant Phenomics*, *2022*, Article 9768502. https://doi.org/10.34133/2022/9768502

SUPPORTING INFORMATION

Additional supporting information can be found online in the Supporting Information section at the end of this article.

How to cite this article: Van Haeften, S., Smith, D., Robinson, H., Dudley, C., Kang, Y., Douglas, C. A., Hickey, L. T., Potgieter, A., Chapman, S., & Smith, M. R. (2025). Unmanned aerial vehicle phenotyping of agronomic and physiological traits in mungbean. *The Plant Phenome Journal*, *8*, e70016. https://doi.org/10.1002/ppj2.70016